EUROPEAN COMMISSION
5th EURATOM FRAMEWORK PROGRAMME 1998-2002
KEY ACTION : NUCLEAR FISSION

HTR-E

High-Temperature Reactor Components and Systems

CONTRACT N°
FIKI-CT-2001-00177

Delivery D31 - Workpackage 4
1.2 Feasibility Study of a Rotating Seal System
1.2.2 Canned Magnetic Bearing

University of Applied Sciences Zittau/Görlitz

GERMANY

Dissemination level: RE
Document N°: HTR-E-04/01-D-4-1-2-1
Status: Final
Delivery No.: D31

HOCHSCHULE ZITTAU/GÖRLITZ (FH) - University of Applied Sciences

Ref.: HZG-IPM 610334/4/2.01/E

DELIVERY D31 (Workpackage 4)

Task 1.2 Feasibility Study of A Rotating Seal System
Subtask 1.2.1 Canned Magnetic Bearing

Authorised administrative official: Dr.-Ing. P. Reinhold
(Chancellor)

Signature

Authorised contact person: Prof. Dr.-Ing. F. Worlitz
(Project Leader)

Signature

Zittau, 01/29/2004

Zu erreichen:
Theodor-Körner-Allee 16 • 02763 Zittau
Tel.: (0 35 83) 61 0
Fax: (0 35 83) 51 06 26
Internet: http://www.hs-zigr.de

Modifications

Revision	Date	Modifications
A	01/29/2004	First Issue
B	03/01/2004	Review by S2M

Summary

The document contributes to the 5th PCRD HTR-E Work package 4, Delivery D31 – Feasibility Study of a Rotating Seal System. It describes the results of the subtask “Canned Magnetic Bearings”.

Characteristic fields of an axial magnetic bearing were calculated and measured. The aim of the analysis was to determine the reduction of forces due to the can material, which leads to an additional resistance in the magnetic circuit.

Contents

1. Introduction/Objectives

The document contributes to the 5th PCRD HTR-E Workpackage 4, Delivery D31 – Feasibility Study of a Rotating Seal System. It describes the results of the subtask "Canned Magnetic Bearings".

The operation of magnetic bearings in High Temperature Reactor Components has special requirements on the design of the bearings, due to

- high temperature
- helium environment

The application of canned magnetic components is one approach to meet these requirements.
Due to the additional can in the magnetic circuit the forces are smaller than in normal case. The objective of the single effects analysis is the estimation of the magnetic forces of canned magnetic bearings. By the example of an axial magnetic bearing the forces are compared to the forces of the same bearing without can material.

The forces are represented in characteristic fields which show the magnetic forces as a function of the air gap and the coil current. At first, the characteristic fields were calculated with finite element software. In a second step the characteristic fields of both cases were measured.

The used inputs are based on the following documents:

- [1] Framatome ANP (FRA): HTR-E – Helium rotating seal – state of art and specifications
- [2] S2M: HTR-E WP4 Task2-1 Canned Magnetic Bearing, Presentation at WP-Meeting in Zittau, Nov. 2002
- [3] Le-Trung,A; Internal Report, Uni-Zittau-Görlitz, 2002
- [4] Kasarda, M.E.F.; Allaire, P.E.; Norris, P.M.; Maslen, E.H.; Mastrangelo, C. Comparison of Measured Rotor Power Losses in Homopolar and Heteropolar Magnetic Bearings, Proceedings of MAG'97, Aug. 1997; Alexandria, VA

2. Investigations of canned magnetic bearings

2.1 Requirements concerning magnetic bearings

The requirements for magnetic bearings for both GT-MHR and PBMR are shown in Table 1. The shown data are based on the following document: Framatome ANP (FRA): HTR-E – Helium rotating seal – state of art and specifications [1].

PARAMETER	GT-MHR	PBMR
Operating pressure	26 bar	26 bar
Operating Temperature	110°C	110°C
Design Temperature	150°C	150°C
Trip Speed	3600 rpm	4200 rpm

Table 1: List of required design parameter

2.2 Properties of canned bearings

One approach to meet the requirements, described in table 1, is the application of canned magnetic bearings. Such bearing type contains an additional can inserted in the bearing gap. Due to the mechanical protection, canned bearings are suitable for the operation in a high pressure or high temperature environments. Further, sensitive bearing parts are not in contact with aggressive environment. But on the other hand the can is an additional resistance in the magnetic circuit. This leads to reduction of the available magnetic forces. Optimal design of bearing is required to keep the force reduction as low as possible. Ideal electromagnetic properties of the can material are the following:

- To avoid unwanted magnetization in the can the relative permeability of the material should be one: $\mu_r=1$
- The electrical conductivity should be as low as possible to keep eddy currents low: $\kappa \to 0$

This are ideal material properties, the real materials values should be as close as possible.
Beside the electro-magnetic properties, the can material must be gas-tight and pressure-tight.

2.3. Survey of can materials

For the selection of a suitable housing material, an overview was developed which type of material are usually used in canned motor pumps. The materials used there can be divided in two main groups: Metals und Plastics. Tables 2 and 3 give an overview about materials in different pump types. Mainly stainless and acid proof steel are used in industrial applications. For our own experiments we used a can material with the number 2.4605 which is similar to (Hastelloy C4) 2.4610

Mat.-No.	Abbreviation	Code
1.4435	X2CrNiMo 18 14 3	
1.4439	X2CrNiMoN 17 13 5	AM
2.4602	NiCr21Mo14W	Hastelloy C 22
2.4610	NiMo16Cr16Ti	Hastelloy C 4
2.4617	NiMo28	Hastelloy B 2
2.4819	NiMo16Cr15W	Hastelloy C 276
2.4669	NiCr15Fe7TiAl	Inconel X 750
3.7035	Ti 99,7	Titan Gr. 2

Table 2: Types of Metals/Alloys used in canned-motor pumps

Name	Abbreviation
Polypropylen	PP
Polytetrafluorethylen	PTFE
Polyethylene	PE

Table 3: Types of plastic materials used in several canned-motor pumps

2.4 Survey of magnetic bearings types

Active magnetic bearings can be divided in two versions:

- Heteropolar bearings
- Homopolar bearings

The hetero polar bearing is characterized by flux lines which are oriented lateral to the rotor axis. That implies a change of polarity of the magnetic field during rotation. The rotor must be laminated to reduce hysteresis and eddy current losses. A hetero polar bearing is designed similar as a conventional electric motor; therefore the structure is much simpler, since existing standard components can be used.

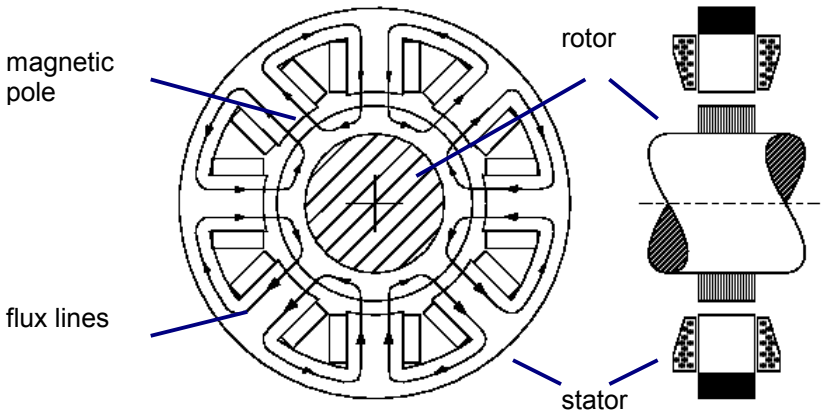

Fig. 1: Heteropolar radial bearing

The flux lines of a homopolar bearing are oriented in direction of the rotating axis. That implies that no change of polarity occurs during the rotation. Therefore no eddy current and hysteresis losses occur. The lamination of the rotor is not necessary.

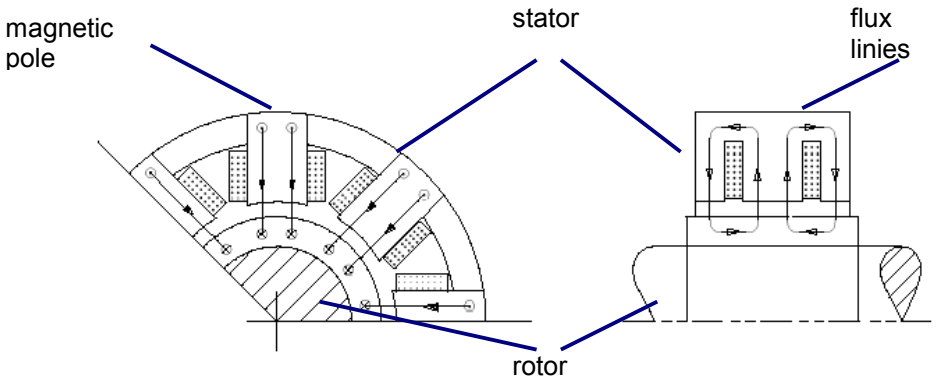

Fig. 2: Homopolar radial bearing

Under the aspect of the loss minimization the homopolar bearing is more suitable. This reflects itself also in experimental results. At a test stand the losses of a homopolar and of a heteropolar bearing were determined. In the case of same flux density of 0.6T in the air gap and in the case of the same speed of 20000 rpm the following bearing losses were reported [3,4]:

- Homopolar bearing: ca. 250 Watt
- Heteropolar bearing: ca. 750 Watt

Our own estimations confirm these results.

3. Single effect analysis at a canned axial magnetic bearing

The objective of the single effect analysis was the estimation of the reduced magnetic forces due to the magnetic resistance of the additional can material.

3.1 Description of the test rig

An existing axial magnetic bearing was modified for the investigation of the can `s influence on the magnetic circuit. Figure 3 shows a cross-section of the axial magnetic bearing in original state. It consists of two circular coils as stationary part, and a rotating disc connecting with the shaft. The nominal air gap is 1mm.

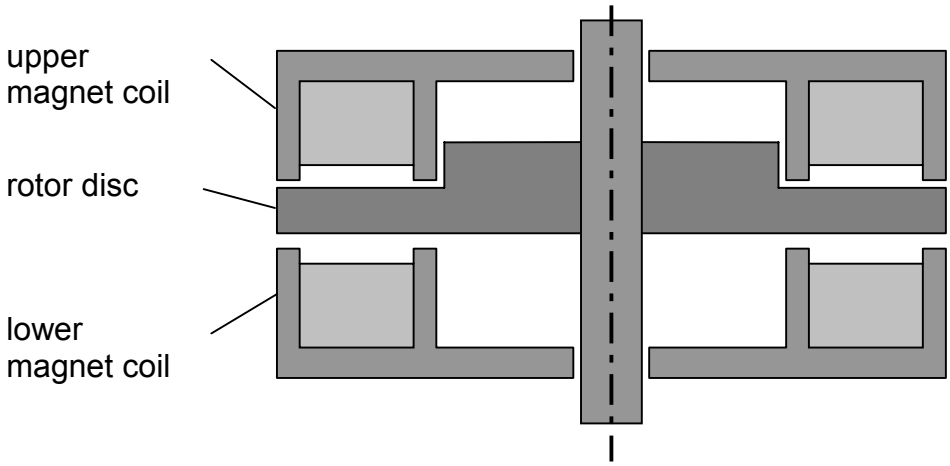

Fig. 3: Test rig axial bearing

Figure 4 shows the modified bearing. For the experimentally investigation two can rings were inserted. The rings are made of stainless steel (Nicrofer 5923 hMo - alloy 59, material number: 2.4605) with a thick of 0.5 mm.

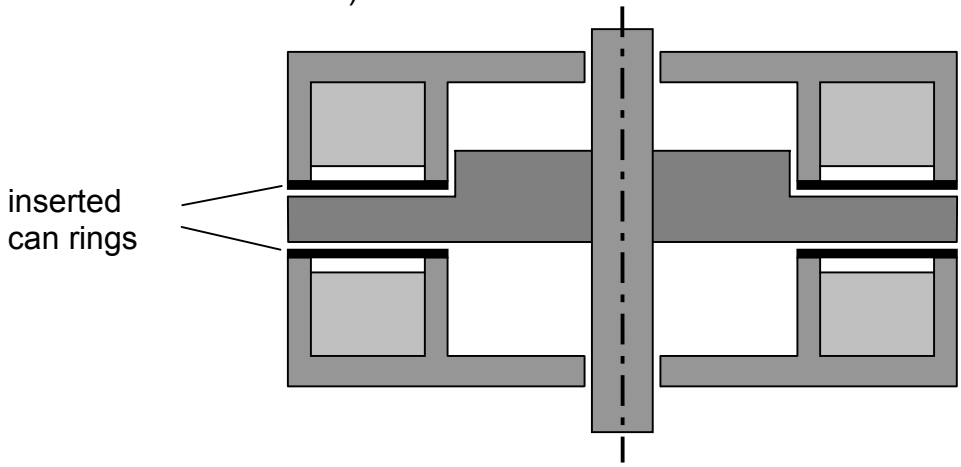

Fig. 4: Modified axial bearing (AMB) with additional can material

The most important electrical and magnetic properties of the can material are shown in Table 4.

Relative Permeability	**Conductivity**
<1.001	0.79 Sm/mm2 at 20°C

Table 4: Material properties of Nicrofer 5923 hMo - alloy 59 (2.4605)

The can's magnetic properties are comparable to the magnetic properties of air and the electrical conductivity is about one order of magnitude less than steels' conductivity.

3.2. Calculation of the Force – Current – Position – Characteristic Field with Finite Element-Models (FEM)

With the FEM-Program *'FEMM'* was calculated the Characteristic Fields of both the axial magnetic bearing in original state and with additional can material. The characteristic field shows the axial force as a function of the coil current and the air gap (i.e. the rotor position). Figure 5 show two cross-sections of the FEM-calculations.

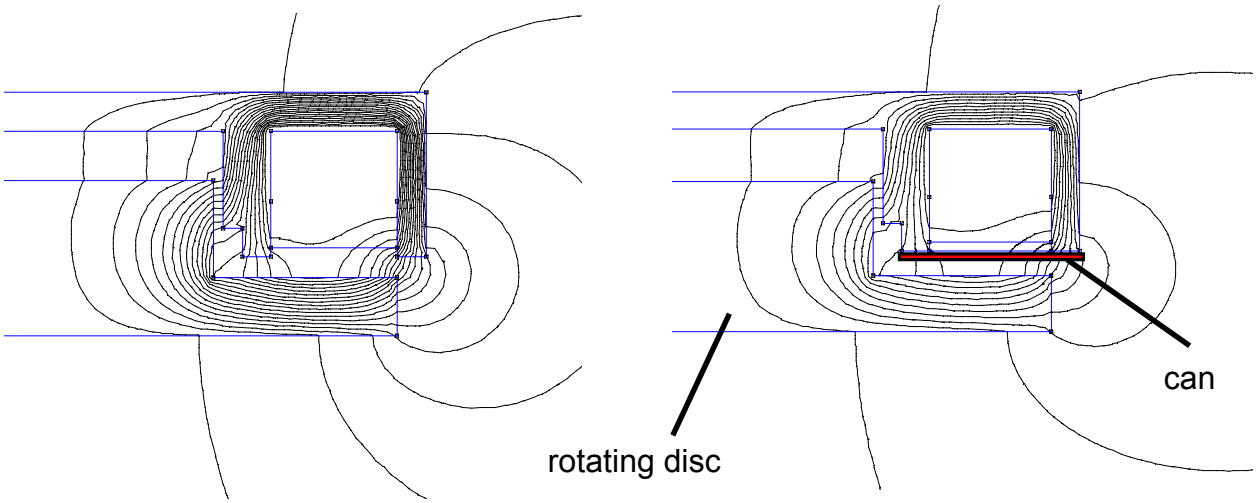

Fig. 5: Example of the flux lines distribution in the axial bearing: left side: original bearing, right side: bearing with additional can

The rotor positions were chosen from -1mm to 1mm in 0.5mm steps. The current range was calculated from 0 Amps to the maximum current of 3 Amps in steps of 0.5Amps.

In Figures 6 and 7 the calculated characteristic fields of both cases are shown. The calculated values can be found in the appendix in Tables 12 and 13.

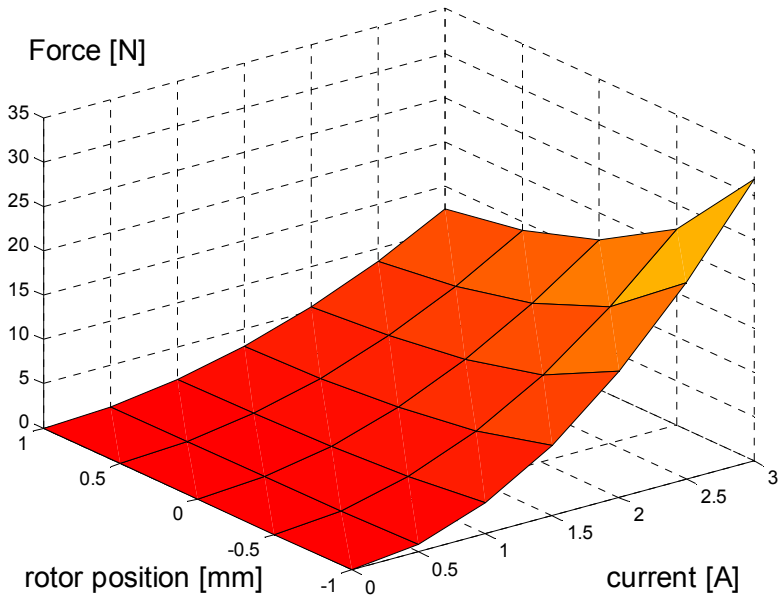

Fig. 6: Calculated characteristic field of the axial bearing original condition

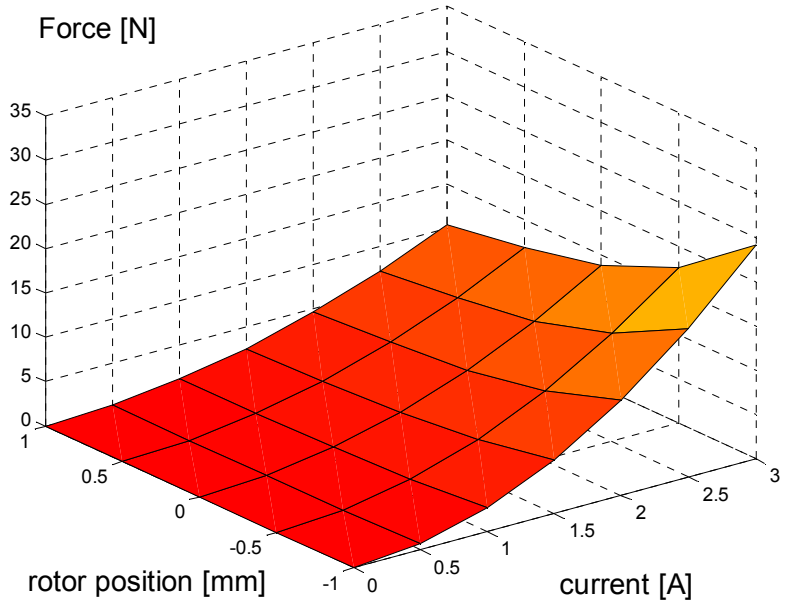

Fig. 7: Calculated characteristic field with can material (Mat. No. 2.4605)

Beside the qualitative similarity it is to recognize that the value of the force at same position in the characteristic field with can material is about 75% - 85% of the original value. Especially in the operating point the Force is reduced to 80 % due o the increased magnetic gap

3.3. Experimental determination of the characteristic fields

3.3.1 Data acquisition

The measurement of the characteristic field-data was done by inserting external axial forces on the rotor. If the shaft position is constant, then the current is only a function of the axial force. The complete characteristic field was measured by means of variation of the rotor shaft position. It is important to note that the measurement was only possible within the catcher bearings bounds. That is the reason for a smaller position range from -0.35mm to +0.3mm, compared to the calculated range. The figure 8 shows the measured characteristic field of the bearing in original state while figure 9 shows the characteristic field of the bearing with additional can material. All the measured values can be found in Tables 14 and 15 in the appendix.

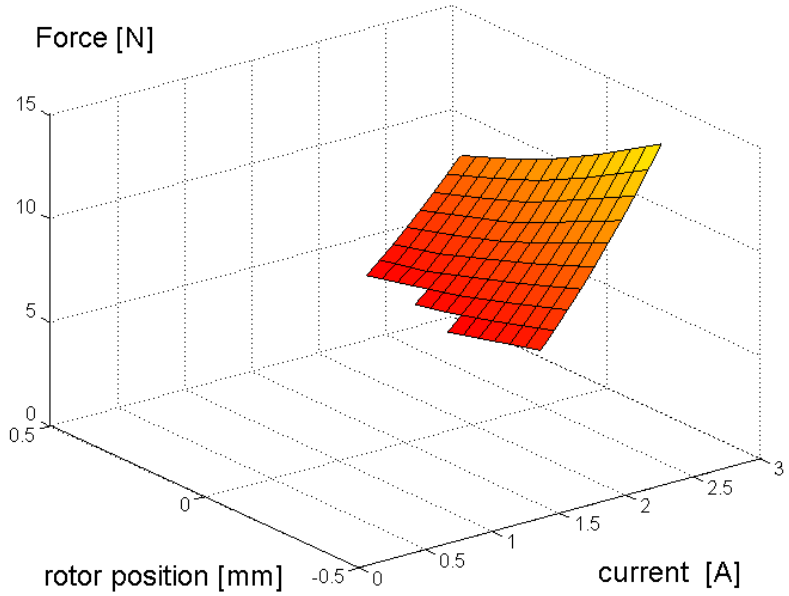

Fig.8: Measured data of the characteristic field: axial bearing in original state

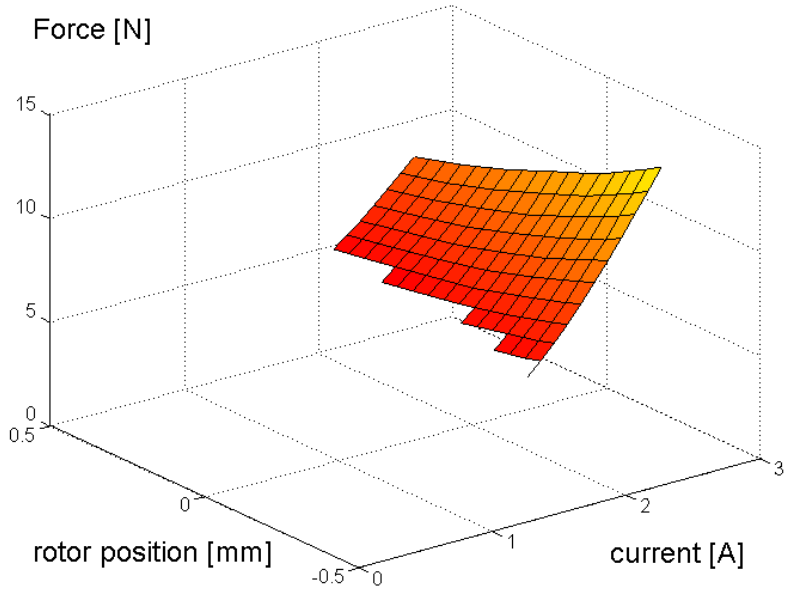

Fig. 9: Measured data of the characteristic field: axial bearing with can material

3.3.2 Simulation Calculations for Verification of Experimental Tests

Force-current-displacement characteristics, verificated by FEM calculations and experimental tests, were integrated in a simulation tool to calculate the behaviour of the magnetic bearing control loop. The objective of the calculations was to verify the results of the experimental tests at the axial magnetic bearing test facility. Similarly to the experiments axial loads and set-points of displacement were varied and calculated coil-currents were saved. Fig. 10 shows the calculated forces of the upper axial bearing coil vs. the axial loads and the set-points of displacement in origin state (without can

material). The axial loads are acting in direction of weight in a range of 0...10 N. The set-points of displacement were varied in a range between the catcher bearing clearance of ±0.5 mm.

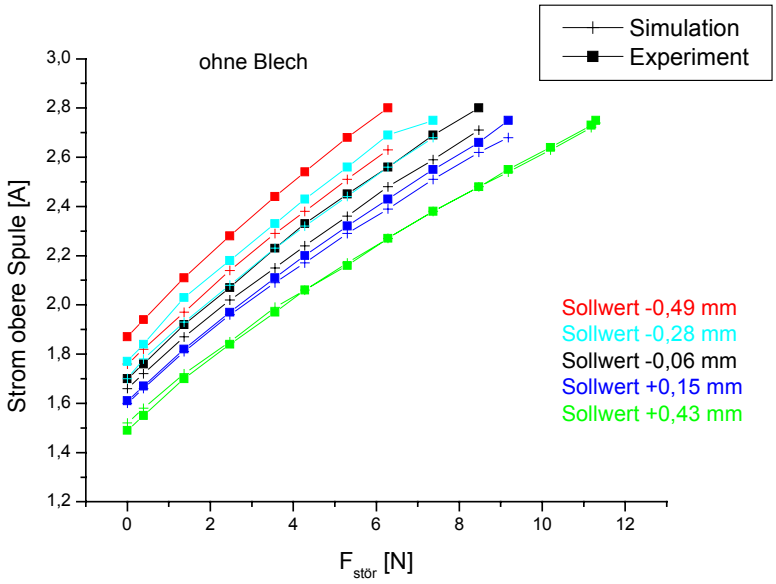

Fig. 10: Coil current vs. axial load and set-point of displacement (without can material)

The maximal relative error between the measured and calculated coil-current amounts 7.1% at the set-point of –0.49mm (lower catcher bearing position). The cause of this error is the difference of the force-current-displacement characteristics determined by FEM calculations and experimental tests.

Fig. 11 shows the calculated forces of the upper axial bearing coil vs. the axial loads and the set-points of displacement with can material. The maximal relative error between the measured and calculated coil-current amounts -3.9% at the set-point of +0.79mm.

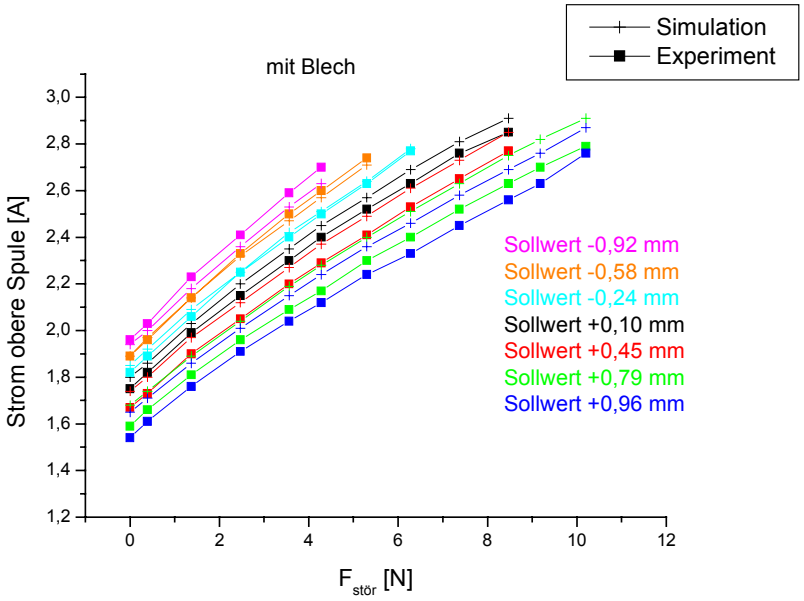

Fig. 11: Coil current vs. axial load and set-point of displacement (with can material)

3.4. Test of Controller Algorithm

3.4.1 Objective

The objective of the investigations in controller algorithm was to determine the behaviour of the AMB control loop by using canned bearings.

Especially interesting was to investigate in standard controller algorithms to proof their applicability or limits and restrictions on these bearings.

3.4.2 Canned Magnetic Bearing Application

The control algorithms were tested on a canned AMB application (rotating wheel) as shown in Fig. 12. The parameters of this application are given in section 3.4.4.

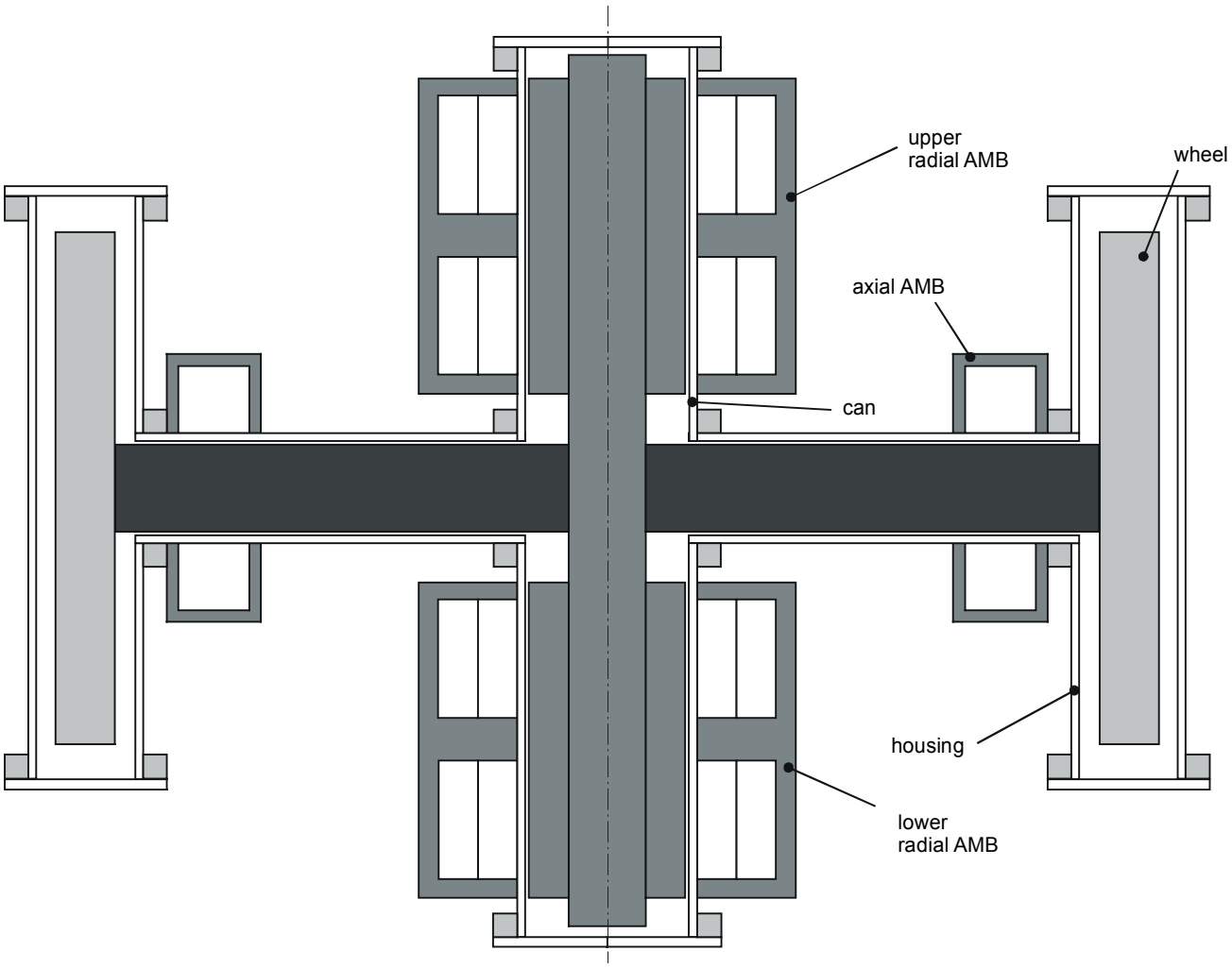

Fig. 12: Canned AMB Application

3.4.3 Simulation Tool MLDyn

The test of the controller in a canned AMB loop was performed with the simulation tool *MLDyn*. *MLDyn* was especially developed for theoretical investigations in the field of active magnetic bearing systems. It contains all components of the AMB control loop (Fig. 13).

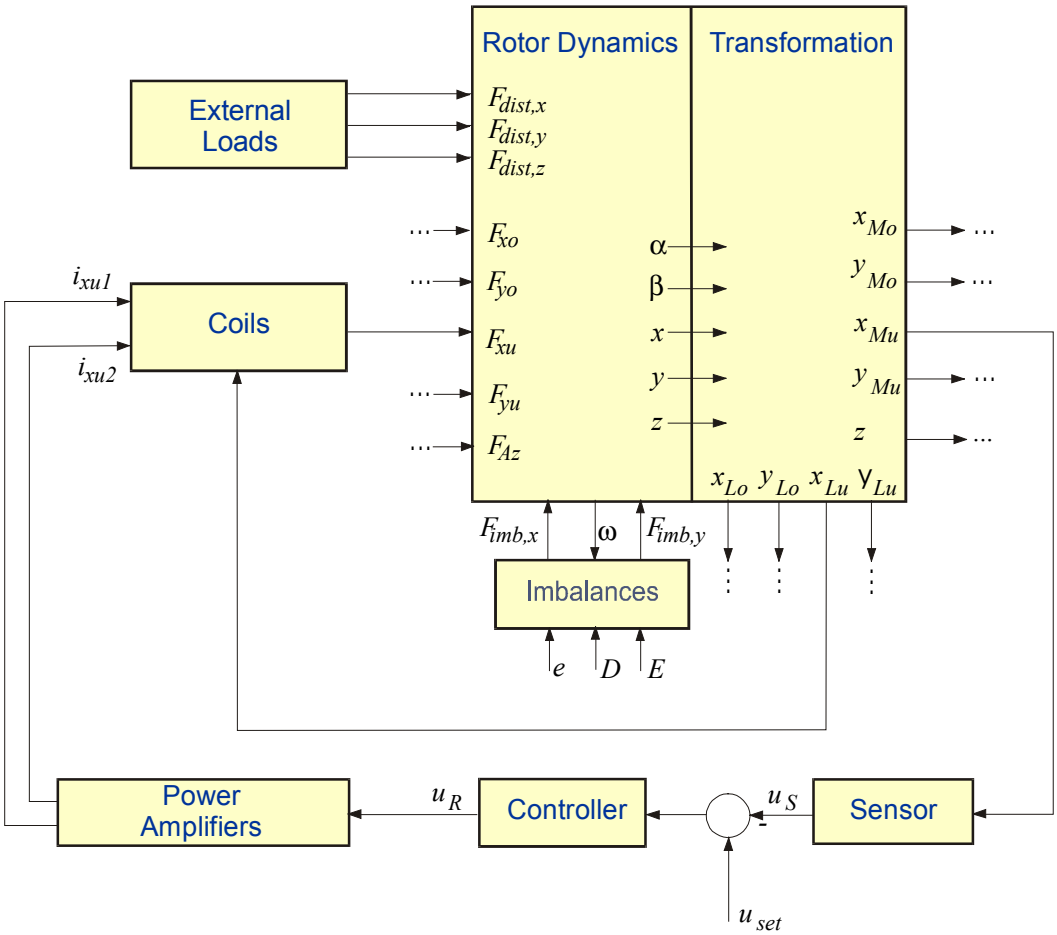

Fig. 13: Structure of the simulation tool *MLDyn*

The simulation tool is characterized by
- modelling the magnetic bearing control loop for completely active magnetically supported rigid rotors,
- a modular type of construction and an easy exchange of components of the control loop,
- emergency operation for imbalances and unit loads,
- the possibility of configuration for any magnetic bearing systems by adjustment of characteristic parameters and structures,
- Verification at pilot plants.

Application fields are
- investigations of the dynamics of rotors,
- loop investigations (transients, numbers of revolutions, critical operating situations, start-up and shut-down operations),
- investigations of the control loop stability,
- support in controller design,
- Preparation of experiments.

3.4.4 Parameterization

Every module of the simulation tool has been parameterized.
Tables 1...5 give an overview about the main parameters of canned AMB application.

Parameter	Symbol	Unit	Value
mass of rotor	m_R	kg	22,9
centre of gravity	a_S	m	0,105
radial moment of inertia	J_{rad}	kg m^2	0,170
axial moment of inertia	J_{ax}	kg m^2	0,289
eccentricity	e	m	1µm (balancing quality Q2,5)
upper radial bearing level	$a_{L,o}$	m	0,17
upper radial sensor level	$a_{M,o}$	m	0,17
lower radial bearing level	$a_{L,u}$	m	0,04
lower radial sensor level	$a_{M,u}$	m	0,04
axial bearing level	a_A	m	0,105

Table 5: Parameters of rotor dynamics module

Parameter	Symbol	Unit	Value
Gain	k_S	V/mm	20
time constant	T_S	s	$8*10^{-6}$

Table 6: Parameters of sensors

Parameter	Symbol	Unit	Value
Gain	k_{UI}	A/V	2
pulse frequency	f_P	kHz	50
max current	I_{max}	A	10
voltage (intermediate circuit)	U_{ZK}	V	100
bias current	I_0	A	5

Table 7 Parameters of power amplifiers

Parameter	Symbol	Unit	Value
time constant	T_{Sp}	s	0,0001 (in set-point position)

Table 8: Parameters of coils

Parameter	Symbol	Unit	Value
air-gap upper radial AMB	s_o	mm	2,7 (incl. can with μ_r=1)
air-gap lower radial AMB	s_u	mm	2,7 (incl. can with μ_r=1)
air-gap axial AMB	s_A	mm	2,7 (incl. can with μ_r=1)

Table 9: Parameters of AMB force module

Based on the input parameter of the coils the force-current-gap characteristic fields of the radial and axial magnets are calculated for the module „coils“ of the simulation tool (Fig. 14 and 15). The radial AMB's have a load capacity of 100 N at nominal air gap and maximum current of 10 A. The starting capacity of the radial bearings is 70 N at maximum air gap (at catcher bearing position).

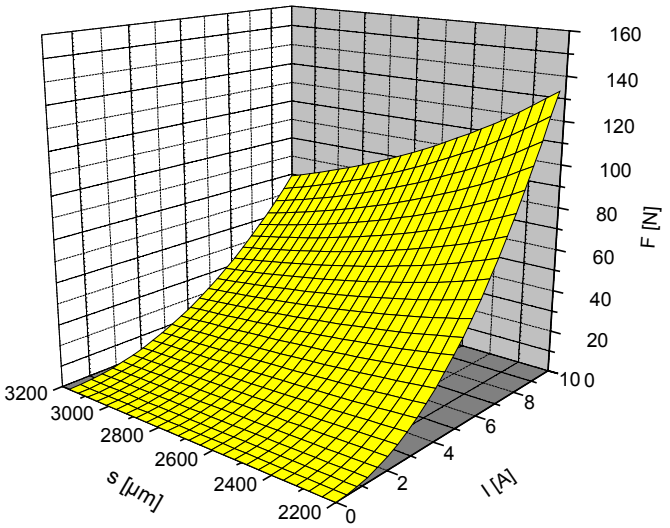

Fig. 14: Characteristics field of radial AMB's (one quadrant)

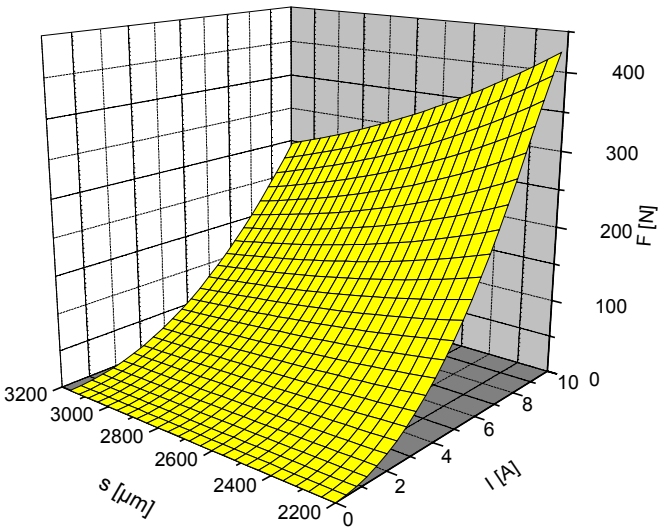

Fig 15: Characteristics field of axial AMB (one coil)

3.4.5 Controller optimization and simulation

3.4.5.1 Basic assumptions for optimization

At the optimization process the parameters of the used PID controllers are adapted with help of simulation calculations.
Optimization will be performed with respect to the disturbance behaviour as the unbalance loads have an essential effect to the operation of an active magnetic bearing.

Quality criteria will be used for controller tuning based on the tests (Table 10). Aim of the optimization is the minimization of these criteria primarily the main criteria.

The following tests will be used
- speed levels and unbalance loads (sinusoidal disturbance)
- start up (rotor lift-up)

	Quality Criteria	
Simulation	**Main Criterion**	**Secondary Criterion**
speed levels and unbalance loads	amplitude of rotor displacement	-
start up	Overshoot	rise time and settling time

Table 10: Quality criteria for controller optimization

3.4.5.2 Start-up

At the start-up operation the shaft must be lifted from an arbitrary position in the catcher bearings to the setpoint position (mainly centre position). A minimal overshoot and a short settling time are required.

The catcher bearing clearance amounts ± 0,5 mm for both the radial bearings and the axial bearing. To avoid a contact between rotor and catcher bearing the overshoot must be less then 80% of the catcher bearing clearance. Fig. 16 shows the overshoot resp. the rise time and settling time vs. the controller gain K_R. In Table 11 the corresponding optimal values of the controller gain regarding the quality criteria. There is to compromise between the fulfilments of all criteria. Main criterion is the minimization of the overshoot $h_{Ü}$. Controller gains k_R >0.6 are not practicable to avoid overshoot $h_{Ü}$ > 400 µm.

y_o	K_{Ryo} optimal	$h_Ü$ [µm]	T_{an} [s]	T_{aus} [s]
Minimum $h_Ü$	0,4	360,69182	0,0101	0,1854
Minimum T_{an}	1,4	452,74499	0,0096	0,2366
Minimum T_{aus}	0,6	391,18754	0,0098	0,17375
y_u	K_{Ryu} optimal	$h_Ü$ [µm]	T_{an} [s]	T_{aus} [s]
Minimum $h_Ü$	0,4	360,71427	0,0101	0,18535
Minimum T_{an}	1,4	452,76159	0,0096	0,23655
Minimum T_{aus}	0,6	391,21624	0,0098	0,1738
x_o	K_{Rxo} optimal	$h_Ü$ [µm]	T_{an} [s]	T_{aus} [s]
Minimum $h_Ü$	0,4	360,69182	0,0101	0,1854
Minimum T_{an}	1,4	452,74499	0,0096	0,2366
Minimum T_{aus}	0,6	391,18754	0,0098	0,17375
x_u	K_{Rxu} optimal	$h_Ü$ [µm]	T_{an} [s]	T_{aus} [s]
Minimum $h_Ü$	0,4	360,71427	0,0101	0,18535
Minimum T_{an}	1,4	452,76159	0,0096	0,23655
Minimum T_{aus}	0,6	391,21624	0,0098	0,1738
z	K_{Rz} optimal	$h_Ü$ [µm]	T_{an} [s]	T_{aus} [s]
Minimum $h_Ü$	0,2	1,56034	0,0567	0,0902
Minimum T_{an}	3,2	140,40848	0,0107	0,75495
Minimum T_{aus}	0,2	1,56034	0,0567	0,0902

Table 11: Optimal Controller Gain in depence of quality criteria

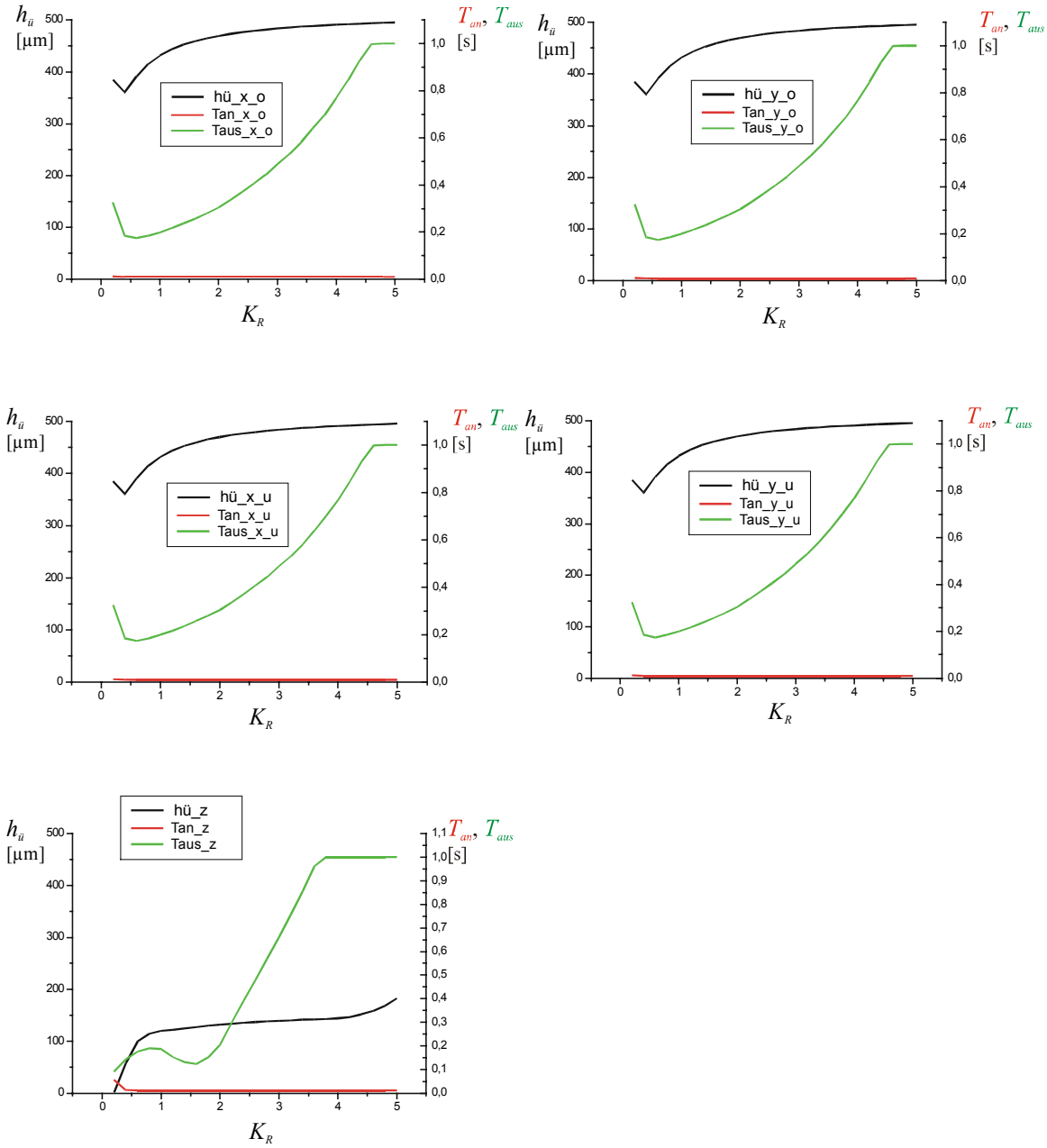

Fig. 16: Overshoot $h_{ü}$ resp. Rise Time T_{an} and Settling Time T_{aus} vs. Controller Gain K_R for Upper (Index o) and Lower (Index u) Radial AMB resp. Axial AMB (Index z)

3.4.5.3 Speed Levels and Unbalance Loads

High loads at the shaft can occur due to resonances vibrations at critical speeds. The reason for these vibrations is unbalances. The unbalances are caused by the eccentricity of the centre of gravity and deviation moments. The arising force is proportionally to the square of the rotational speed.

Fig. 17 shows the maximum amplitude of rotor position and the bearing force vs. the controller gain and the rotational speed exemplarily for the radial AMB's in x-direction.

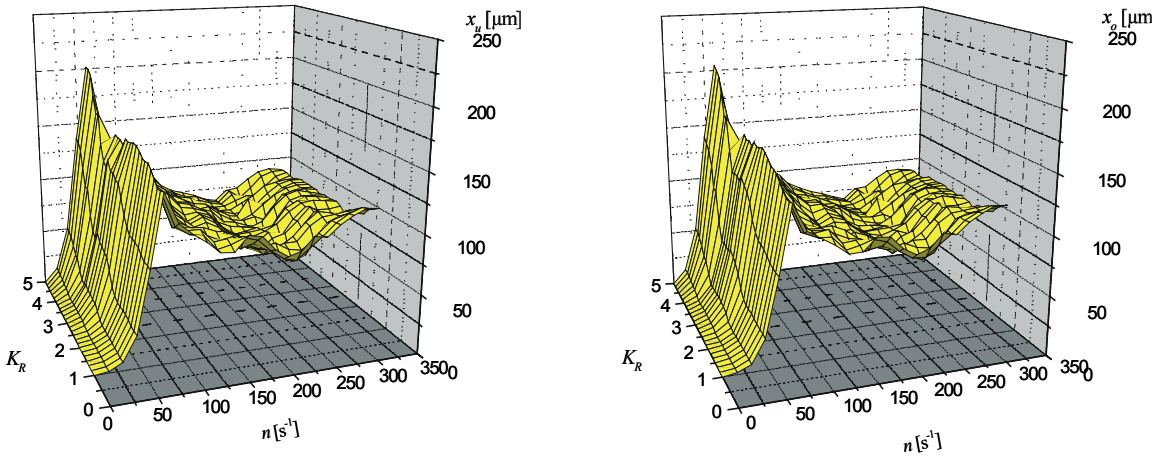

Fig. 17: Maximum Amplitude of Rotor Position and the Bearing Force vs. Controller Gain and Rotational Speed

The amplitude of rotor position varies with the controller gain and the rotational speed. Increased amplitudes occur at the nominal speed of 80 s^{-1} (4,800 rpm) but the radial AMB's are able to react the loads caused by unbalances up to full speed (20,000 rpm).

Fig. 18 shows the result of investigations to determine an optimal controller gain where the amplitude of rotor position is minimized at all rotational speed. The gain must be varied in wide range to reach a minimum rotor displacement.
Therefore it is advantageous to apply controllers where the gain is adapted dependent on the speed.

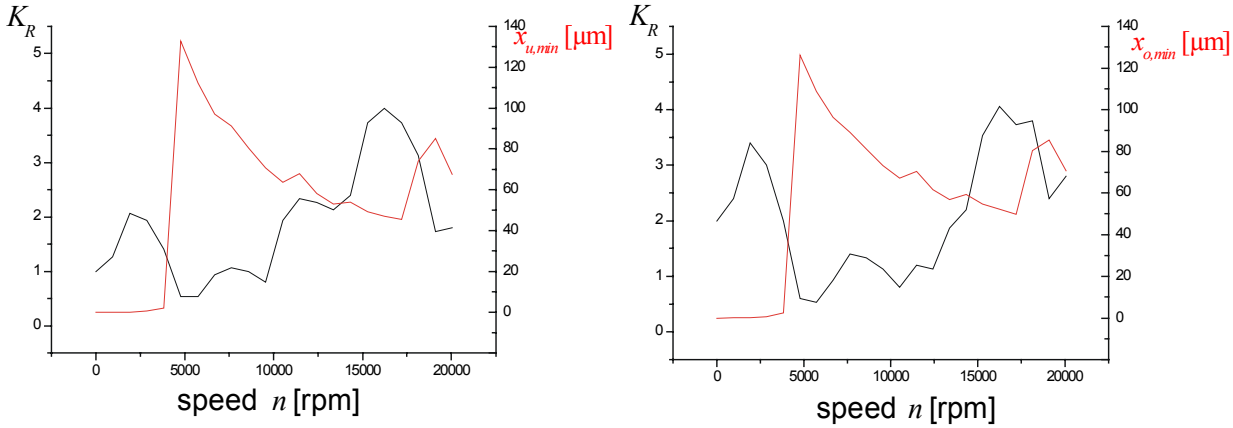

Fig. 18: Minimum Amplitude of Rotor Position for Full Speed Range and Optimal Gain

3.4.6 Conclusions

Standard PID controller has been tested at a canned AMB application. With respect to the fulfilment of the quality criteria this controller can also be used for canned bearings. However, note that a smaller stability range of gain is available due to the can and the higher gap between stator and rotor. Furthermore a wide range of gain adaptation is necessary to reach minimal rotor displacement in comparison to an application without can.

3.5 FE-Calculation of the influence of the relative permeability

The influence of the permeability to the magnetic force was studied at a model of an axial magnetic bearing with can material. The axial force as a function of the permeability was calculated with FEM-program. All the geometric data and the current in the coil were kept constant in the example in Figure 19. Only the relative permeability μ_r was changed from μ_r =1…100.

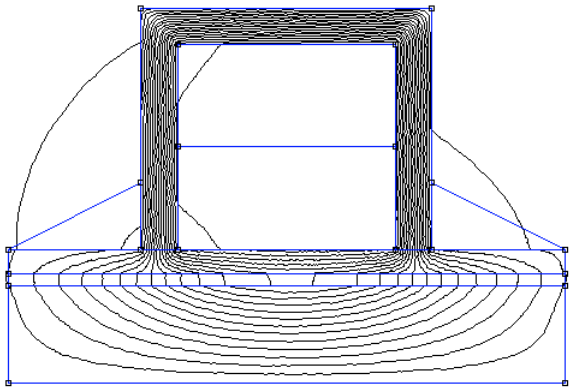

Fig. 19: Measured data of the characteristic field: axial bearing with can material

The calculations results in Figure 20 shown, that there is a permeability number, where the axial force is maximum. The force maximum is at a relative permeability of μ_r = 10.

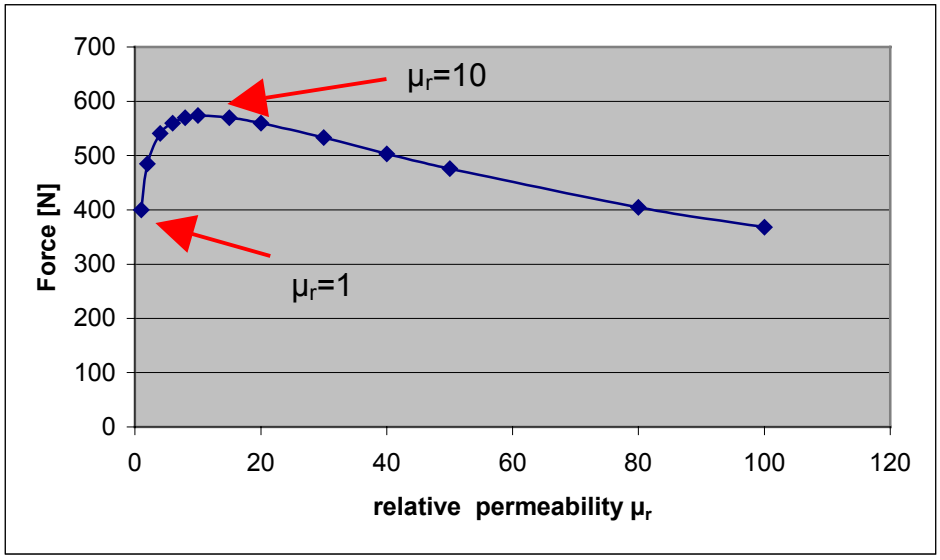

Fig. 20: Axial force as function of the magnetic property of the can material

This effect can be explained by two opposite tendencies: At a permeability of $\mu_r = 1$ the can act as enlarged gap. With increasing permeability decreases the magnetic gap width and leads to increasing forces. But at permeability of $\mu_r >> 1$ the flux leakage between the magnet poles and the can material increases. The can forms a magnetic shortcut between the magnetic poles. Therefore, the axial force of the bearing is reduced by relative permeability of $\mu_r >> 10$.

The magnetic properties of can's material have a significant factor on the magnetic circuit and on the resulting forces. There is an optimum relative permeability, but it depends also on the bearing geometry, which was not part of this investigation.

3.6 FE – Calculation of Canned Radial Bearing

With the results of the previous studies a canned radial bearing was calculated. The radial bearing is a homo-polar type and consists of four coils. The bearing was designed for a rated force of 75 N. The coils are divided in excitation coil and control coil. In Figure 21 different operating states of the radial bearing are shown:

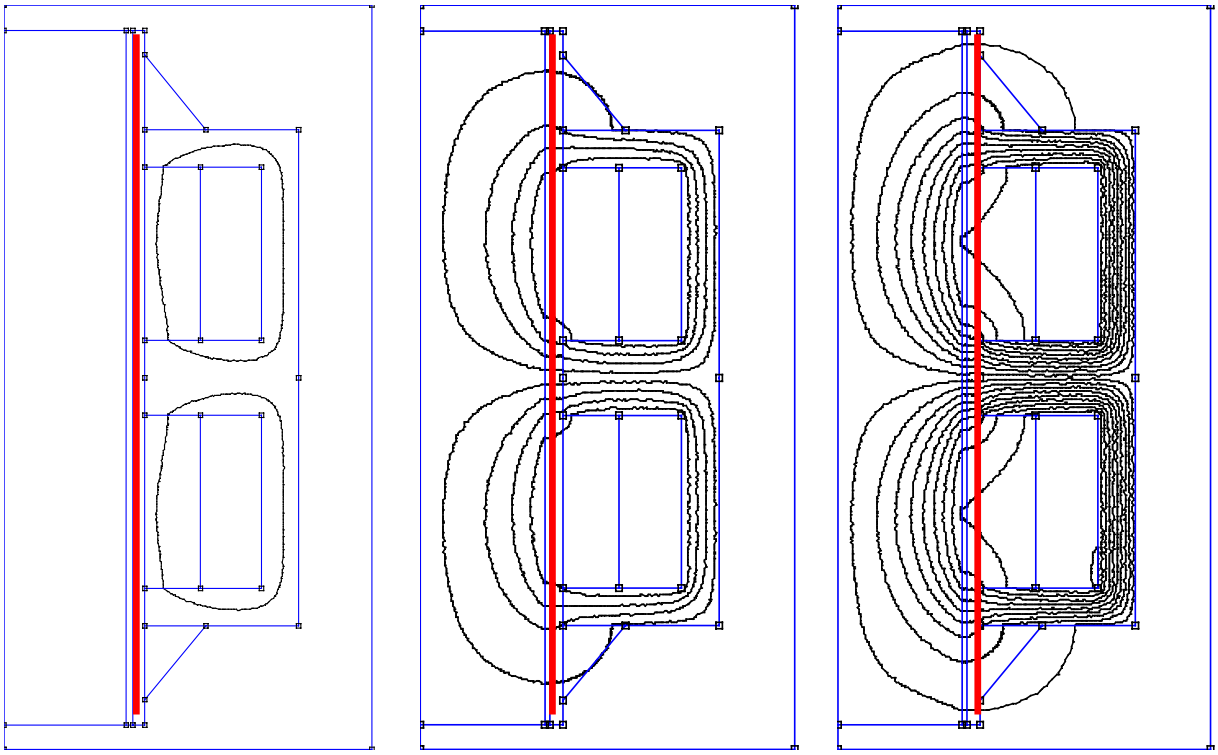

Fig. 21: Different operating states of the radial bearing: The excitation coil current and control coil current are in opposite direction (left part); exitation current only (center part); unidirectional (right part)

4. Conclusions

The investigation reported here was a very basic approach two the subject of canned bearings in High Temperature Reactors. It proofs the basic functionality of a magnetic bearing with a can on the stator part of the bearing. The value of the force at same position in the characteristic field with can material is about 75% - 85% compared to the original value. Especially in the operating point the Force is reduced to 80 % due o the increased magnetic gap. But this it not a concern as this phenomena can be easily compensated by adding some more turns to the coil. To obtain the same force as in the non-canned case the bearing must be somewhat roomier built.

The measured data were in good accordance with the calculated ones. This shows the applicability of the FEM-Model which can be used for further calculations.

Further, standard PID controller has been tested at a canned AMB application. With respect to the fulfilment of the quality criteria this controller can also be used for canned bearings. The calculations and the experimental data show that is possible to work with the same controller for both canned and non-canned bearings. So it can be said that the dynamic behaviour is not so much affected by the can.

Appendix

Current [A] / Position [mm]	0	0.5	1.0	1.5	2.0	2.5	3.0
-1.0	0	0.88	3.45	7.97	14.17	22.15	31.86
-0.5	0	0.62	2.46	5.54	9.86	15.41	22.18
0	0	0.47	1.88	4.24	7.54	11.79	16.97
0.5	0	0.39	1.56	3.52	6.25	9.77	14.07
1.0	0	0.34	1.37	3.09	5.50	8.59	12.38

Table 12: Calculated characteristic field data of the bearing in original condition as shown in Figure 6

Current [A] / position [mm]	0	0.5	1.0	1.5	2.0	2.5	3.0
-1.0	0	0.67	2.68	6.04	10.75	16.79	24.17
-0.5	0	0.49	1.95	4.39	7.82	12.22	17.59
0	0	0.38	1.54	3.47	6.14	9.60	13.84
0.5	0	0.33	1.32	2.98	5.30	8.28	11.92
1.0	0	0.29	1.16	2.61	4.64	7.25	10.44

Table 13: Calculated characteristic field data of the bearing with can material, as shown in Figure 7

position [mm] / Force [N]	-0.35	-0.15	0	0.15	0.3
5.07	1.49	1.61	1.70	1.77	1.87
5.46	1.55	1.67	1.76	1.84	1.94
6.45	1.70	1.82	1.92	2.03	2.11
7.54	1.84	1.97	2.07	2.18	2.28
8.63	1.97	2.11	2.23	2.33	2.44
9.35	2.06	2.20	2.33	2.43	2.54
10.37	2.16	2.32	2.45	2.56	2.68
11.35	2.27	2.43	2.56	2.69	2.8
12.44	2.38	2.55	2.69	2.75	
13.54	2.48	2.66	2.80		
14.25	2.55	2.75			
15.27	2.64				
16.26	2.73				
16.36	2.75				

Table 14: Measured values of the characteristic field of the bearing without can material as shown in Figure 8

position [mm] / Force [N]	-0.375	-0.3	-0.15	0	0.15	0.3	0.45
5.07	1.54	1.59	1.67	1.75	1.82	1.89	1.96
5.46	1.61	1.66	1.73	1.82	1.89	1.96	2.03
6.45	1.76	1.81	1.90	1.99	2.06	2.14	2.23
7.54	1.91	1.96	2.05	2.15	2.25	2.33	2.41
8.63	2.04	2.09	2.20	2.30	2.40	2.50	2.59
9.35	2.12	2.17	2.29	2.40	2.50	2.60	2.70
10.37	2.24	2.30	2.41	2.52	2.63	2.74	
11.35	2.33	2.40	2.53	2.63	2.77		
12.44	2.45	2.52	2.65	2.76			
13.54	2.56	2.63	2.77	2.85			
14.25	2.63	2.70					
15.27	2.76	2.79					

Table 15: Measured values of the characteristic field of the bearing with can material as shown in Figure 9